

# Observation of Temperature-Induced Crossover to an Orbital-Selective Mott Phase in $A_x\text{Fe}_{2-y}\text{Se}_2$ (A=K, Rb) Superconductors

M. Yi,<sup>1,2</sup> D. H. Lu,<sup>3</sup> R. Yu,<sup>4</sup> S. C. Riggs,<sup>1,2</sup> J.-H. Chu,<sup>1,2</sup> B. Lv,<sup>5</sup> Z. Liu,<sup>1,2</sup> M. Lu,<sup>1,6</sup> Y.-T. Cui,<sup>1</sup>  
M. Hashimoto,<sup>3</sup> S.-K. Mo,<sup>7</sup> Z. Hussain,<sup>7</sup> C. W. Chu,<sup>5</sup> I. R. Fisher,<sup>1,2</sup> Q. Si,<sup>4</sup> and Z.-X. Shen<sup>1,2</sup>

<sup>1</sup>Stanford Institute of Materials and Energy Sciences, Stanford University, Stanford, CA 94305, USA

<sup>2</sup>Departments of Physics and Applied Physics, and Geballe Laboratory for Advanced Materials, Stanford University, Stanford, CA 94305, USA

<sup>3</sup>Stanford Synchrotron Radiation Lightsource, SLAC National Accelerator Laboratory, Menlo Park, CA 94025, USA

<sup>4</sup>Department of Physics and Astronomy, Rice University, Houston, TX 77005, USA

<sup>5</sup>Department of Physics, Texas Center for Superconductivity, University of Houston, Houston, TX 77204, USA

<sup>6</sup>National Laboratory of Solid-State Microstructures and Department of Materials Science and Engineering, Nanjing University, Nanjing 210093, China

<sup>7</sup>Advanced Light Source, Lawrence Berkeley National Lab, Berkeley, CA 94720, USA

(Dated: November 26, 2012)

Using angle-resolved photoemission spectroscopy, we observe the low temperature state of the  $A_x\text{Fe}_{2-y}\text{Se}_2$  (A=K, Rb) superconductors to exhibit an orbital-dependent renormalization of the bands near the Fermi level—the  $d_{xy}$  bands heavily renormalized compared to the  $d_{xz}/d_{yz}$  bands. Upon raising temperature to above 150K, the system evolves into a state in which the  $d_{xy}$  bands have depleted spectral weight while the  $d_{xz}/d_{yz}$  bands remain metallic. Combined with theoretical calculations, our observations can be consistently understood as a temperature-induced crossover from a metallic state at low temperature to an orbital-selective Mott phase (OSMP) at high temperatures. Moreover, the fact that the superconducting state of  $A_x\text{Fe}_{2-y}\text{Se}_2$  is near the boundary of such an OSMP constrains the system to have sufficiently strong on-site Coulomb interactions and Hund's coupling, highlighting the non-trivial role of electron correlation in this family of iron-based superconductors.

PACS numbers: 71.30.+h, 74.25.Jb, 74.70.Xa, 79.60.-i

Electron correlation remains a central focus in the study of high temperature superconductors. The strongly correlated cuprate superconductors are understood as doped Mott insulators (MI) [1] while the iron-based superconductors (FeSCs) have been found to be moderately correlated [2–4]. While the different FeSC families share the common Fe  $3d$  low energy electronic structure, they vary in physical properties such as ordered magnetic moment and effective mass [5]. Electron correlation systematically varies from weak to moderate from the phosphides to the arsenides and to the Fe(Te,Se) chalcogenides, where heavy band renormalization [6, 7] and polaronic behaviors [8] have been observed. However, even in the Fe(Te,Se) family, resistivity remains metallic [9]. The newest chalcogenide superconductors,  $A_x\text{Fe}_{2-y}\text{Se}_2$  (A=alkali metal) [10–14] (AFS), with a large moment of  $3.3\mu_B$  [15], is the first FeSC family to exhibit insulating behavior in its phase diagram, which may suggest stronger correlation for certain doping regime.

Another important factor for understanding the FeSCs is their multi-orbital nature. In such a system, orbital-dependent behavior as well as competition between inter- and intra-orbital interactions could play a critical role in determining their physical properties. Theoretical models have considered correlation effects in the bad metal regime in terms of an incipient Mott picture [5, 16–18], and the proximity to the Mott transition may be orbital-

dependent even for orbitally-independent Coulomb interactions [19, 20]. What arises from the model is an orbital selective Mott phase (OSMP), in which some orbitals are Mott-localized while others remain itinerant. First introduced in the context of the  $\text{Ca}_{2-x}\text{Sr}_x\text{RuO}_4$  system [21], an OSMP may result from both the orbital-dependent kinetic energy and the combined effects of the Hund's coupling and crystal level splittings [22, 23]. An OSMP links naturally with models of coexisting itinerant and localized electrons that have been proposed to compensate for the shortcomings of both strong coupling and weak coupling approaches [24, 25]. However, to date, there has been no experimental evidence for OSMP in any FeSC.

In this Letter, we present angle-resolved photoemission spectroscopy (ARPES) data from two superconducting AFSs,  $\text{K}_x\text{Fe}_{2-y}\text{Se}_2$  (KFS) and  $\text{Rb}_x\text{Fe}_{2-y}\text{Se}_2$  (RFS), with  $T_C$  of 32K and 31K, respectively, as well as insulating and intermediate AFSs (see SI). We observe the superconducting AFSs undergoing a temperature-induced crossover from a metallic state in which all three  $t_{2g}$  orbitals ( $d_{xy}$ ,  $d_{xz}$  and  $d_{yz}$ ) are present near the Fermi level ( $E_F$ ) to a state in which the  $d_{xy}$  bands have diminished spectral weight while the  $d_{xz}/d_{yz}$  bands remain metallic. In addition, the intermediate doping shows stronger correlation than the superconducting doping, as seen in the further renormalization of the  $d_{xz}/d_{yz}$  bands and the much more suppressed  $d_{xy}$  intensity, while the insulating

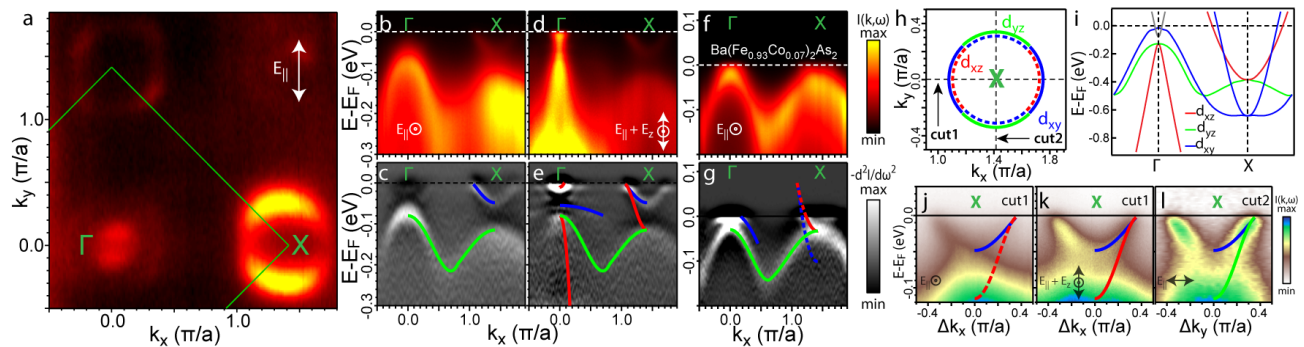


FIG. 1. Electronic structure of  $K_x\text{Fe}_{2-y}\text{Se}_2$ . (a) FS mapping with the 2-Fe BZ boundary marked in green. (b),(d) Spectral images and (c),(e) second derivative in energy along the  $\Gamma$ -X direction. (f)-(g) Similar measurements as (b)-(c) on  $\text{Ba}(\text{Co}_{0.07}\text{Fe}_{0.93})_2\text{As}_2$ . (h) Schematic of the dominant orbital characters of the two electron pockets at X, with one pocket (dotted) imploded for clarity. (i) LDA calculations [29] for KFS. (j)-(l) Spectral images across X under different polarizations and cut directions. All light polarizations are marked. Dominant orbital characters indicated by color: blue ( $d_{xy}$ ), red ( $d_{xz}$ ), green ( $d_{yz}$ ). All data taken at 30 K, with 47.5 eV photons except (d), (e) and (k), which were taken with 26 eV photons. We note very little  $k_z$  dispersion exists in the electron bands [26].

doping has no spectral weight near  $E_F$  in any orbitals. From comparison with our theoretical calculations, the ensemble of our observations are most consistent with the understanding that the presence of strong Coulomb interactions and Hund's coupling place the superconducting AFSs near an OSMP at low temperatures, and crosses over into the OSMP at high temperature, while the intermediate and insulating compounds are on the boundary of the OSMP and in the MI phase, respectively, suggesting the importance of electron correlation in this family of FeSCs.

The low temperature electronic structure of KFS is shown in Fig. 1. The Fermi surface (FS) of KFS consists of large electron pockets at the Brillouin zone (BZ) corner—X-point, and a small electron pocket at the BZ center— $\Gamma$ -point (Fig. 1(a)), consistent with previous ARPES reports [26–28]. For the crystallographic 2-Fe unit cell, LDA calculations predict two electron bands at X [29] (Fig. 1(i)). While FS map appears to show only one pocket at X, measurements under different polarizations (Fig. 1(j)-(l)) reveal the expected two electron bands with nearly degenerate Fermi crossings ( $k_F$ ) but different band bottom positions—a shallower one around -0.05 eV and a deeper one that extends to the top of the  $d_{xz}/d_{yz}$  hole-like band at  $\sim 0.12$  eV. The Luttinger volume of the two electron pockets gives  $\sim 0.16$   $e^-/\text{Fe}$ . Considering that the  $C_4$  symmetry of the crystal dictates the degeneracy between the  $d_{xz}/d_{yz}$  electron band bottom and corresponding  $d_{yz}/d_{xz}$  hole band top at X, the shallower electron band that is clearly not degenerate with the hole band is most likely of  $d_{xy}$  character, and the deeper one  $d_{xz}$  along  $\Gamma$ -X and  $d_{yz}$  along the perpendicular direction (see SI). This orbital character assignment seems to contradict the LDA prediction of the shallower electron band as  $d_{xz}/d_{yz}$  and the deeper one  $d_{xy}$  in FeSC [30], as ob-

served in  $\text{Ba}(\text{Co}_{0.07}\text{Fe}_{0.93})_2\text{As}_2$  (Fig. 1(f),(g)). However, this can be understood if we consider the KFS band structure as a whole. Three filled hole bands are observed near  $\Gamma$  (Figs. 1(d),(e)), where the two lower ones can be identified as  $d_{xz}/d_{yz}$  and the higher one  $d_{xy}$  (see SI). Interestingly, the  $d_{xy}$  band is far more renormalized (a factor of  $\sim 10$ ) compared to LDA than the  $d_{xz}/d_{yz}$  bands (a factor of  $\sim 3$ ), indicating stronger correlation for the  $d_{xy}$  orbital. This is in sharp contrast to the  $\text{Ba}(\text{Co}_{0.07}\text{Fe}_{0.93})_2\text{As}_2$  band structure, in which all orbitals are renormalized by about the same factor ( $\sim 2$ ) compared to LDA. Hence, our assignment of  $d_{xy}$  character to the shallower electron band is consistent with strong orbital-dependent renormalization, which brings the original deeper  $d_{xy}$  electron band at X to be shallower than the  $d_{xz}/d_{yz}$  band. This orbital-dependent renormalization behavior also emerges from our theoretical calculations as will be discussed later.

Next, an interesting phenomenon is observed with raised temperature. Fig. 2(a) shows the electron bands at X under a polarization that has stronger matrix elements for  $d_{xy}$  than  $d_{xz}$  [31]. At low temperatures,  $d_{xy}$  band is clearly resolved with weaker intensity for the  $d_{xz}$  band. With increasing temperature, the spectral weight of the whole  $d_{xy}$  band noticeably diminishes, revealing the remaining  $d_{xz}$  band at high temperatures. In Fig. 2(b), the deeper  $d_{yz}$  band has more intensity than the corresponding  $d_{xz}$  band in Fig. 2(a) while the presence of the  $d_{xy}$  band is still very noticeable from the increased intensity near  $E_F$  where the two bands overlap, as well as from the energy distribution curves (EDCs) shown in Fig. 2(c). With increasing temperature, again, the spectral weight of the whole  $d_{xy}$  band diminishes, revealing the remaining  $d_{yz}$  band at high temperatures, which clearly has a deeper band bottom than the shallower  $d_{xy}$  band. In addition, we have artificially introduced a 210K thermal

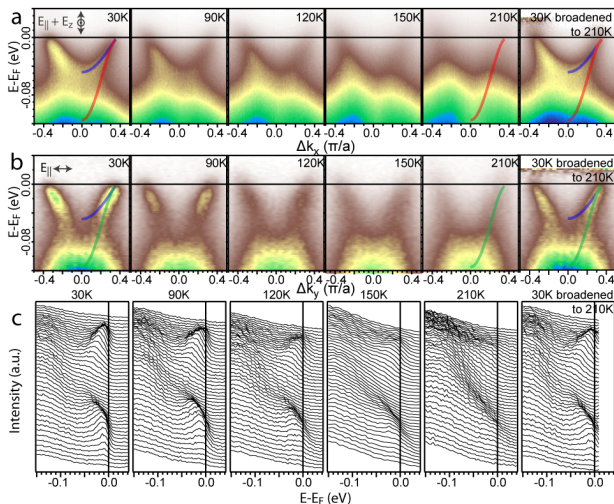


FIG. 2. Temperature dependence of electron bands at X. (a) Spectral images taken with 26eV photons along cut1 as marked in Fig. 1(h). (b) Spectral images and (c) corresponding EDCs taken with 47.5eV photons along cut2. Last column shows the 30K data with an artificially introduced 210K thermal broadening, in comparison to the real 210K data.

broadening to the 30K spectra as shown in the last column of Fig. 2. The clear contrast to the 210K data rules out a trivial thermal broadening as an origin for the observed diminishing of  $d_{xy}$  spectral weight.

To evaluate this behavior quantitatively, we analyze the temperature dependence of the EDCs at the X-point (Fig. 3(c)). At all temperatures, there is a large hump background corresponding to the hole-like dispersion at  $\sim -0.12$ eV. At low temperatures, there is another peak around  $-0.05$ eV corresponding to the  $d_{xy}$  band bottom. We fit these EDCs with a Gaussian for the hump background and a Lorentzian for the  $d_{xy}$  band. The integrated spectral weight for the fitted  $d_{xy}$  peak is plotted in Fig. 3(d), which decreases toward zero with increasing temperature, seen as a non-trivial drop between 100K and 200K. As an independent check against trivial thermal effect, we choose small regions in the spectral image (marked in Fig. 3(a)-(b)) dominated by  $d_{xy}$  (blue),  $d_{yz}$  (green), and mixed  $d_{xy}$  and  $d_{xz}/d_{yz}$  (magenta/cyan) characters and plot their integrated intensities as a function of temperature (Fig. 3(e)). The spectral weight from  $d_{xy}$ -dominated region rapidly decreases, consistent with the fitted result in Fig. 3(d), while that of  $d_{yz}$ -dominated region does not drop in a similar manner. The regions of mixed orbitals show a slower diminishing spectral weight compared to that for  $d_{xy}$ , reflecting the contributions from both  $d_{xz}/d_{yz}$  and  $d_{xy}$  orbitals. Although this method has the uncertainty of small leakage of other orbitals into the chosen regions, which is the likely cause of the finite residual value for the  $d_{xy}$  curve, the contrasting behavior of the  $d_{xy}$  versus  $d_{xz}/d_{yz}$  orbitals is clearly demonstrated. A temperature cycle test was performed

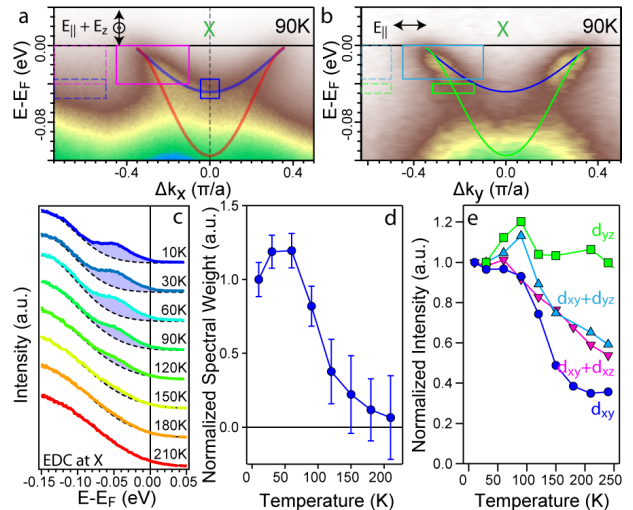


FIG. 3. Temperature dependence analysis. (a)-(b) 90K spectral image of Fig. 2(a)-(b). (c) EDCs at X from (a) for selected temperatures, fitted to a Gaussian background (dotted line) and a Lorentzian peak (shaded region). (d) The integrated Lorentzian spectral weight is plotted against temperature. (e) Temperature-dependence of the averaged intensity of the colored boxes in (a)-(b), with background (dotted box of the same energy window marked by same color) for each box subtracted. The resulting temperature-dependent curve is then normalized by the initial value. The blue (green) region has dominant spectral weight from the  $d_{xy}$  ( $d_{yz}$ ) band, whereas the magenta (cyan) region is of mixed  $d_{xy}$  and  $d_{xz}$  ( $d_{yz}$ ) characters.

to exclude the possibility of sample aging (see SI). Measurements on the sister compound RFS reveal similar behavior (SI), suggesting the generality of this phenomenon in this family of superconductors. This observation of a selected orbital that loses coherent spectral weight while the others remain metallic is reminiscent of a crossover into an OSMP in which selected orbitals become Mott localized while others remain metallic.

To further understand this phenomenon, we perform theoretical calculations based on a five-orbital Hubbard model to study the metal-to-insulator transition (MIT) in the paramagnetic phase using a slave-spin mean-field method [32, 33]. At commensurate electron filling  $n=6$  per Fe (corresponding to  $\text{Fe}^{2+}$  of the parent FeSC), we find the ground state of the system to be a metal, an OSMP or a MI depending on the intra-orbital repulsion  $U$  and the Hund's coupling  $J$ . Furthermore, the MIT can be triggered by increasing temperature (Fig. 4(a)) due to the larger entropy of the insulating phase. At a fixed interaction strength (within a certain range, Fig. 4(a)), the system goes from a metal to an OSMP and then to a MI with increasing temperature. The MI phase is suppressed by electron doping. By contrast, the OSMP can survive, as shown in Fig. 4(b) for  $n=6.15$ , which roughly corresponds to the filling of the superconducting state from ARPES measurements. From the evolution of the

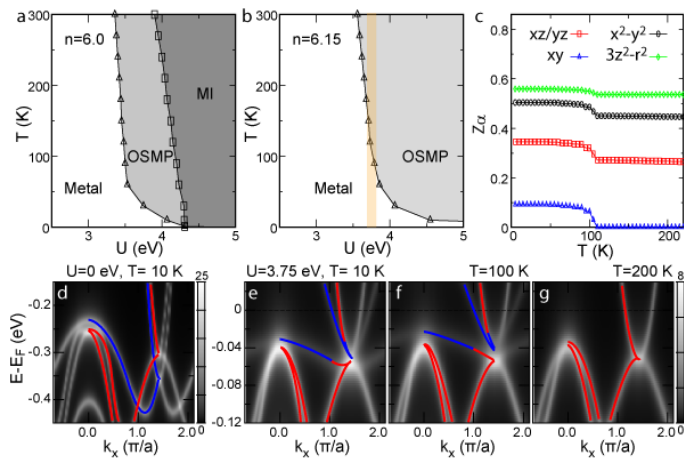


FIG. 4. Theoretical calculation based on a five-orbital Hubbard model. (a)-(b) Slave-spin mean-field phase diagrams of the five-orbital Hubbard model for KFS at  $J/U=0.15$  and two electron densities. OSMP and MI refer to orbital-selective Mott phase and Mott insulator, respectively. (c) The evolution of the orbital-resolved quasiparticle spectral weight  $Z_\alpha$  with temperature at  $n=6.15$ ,  $U=3.75\text{eV}$ , and  $J/U=0.15$ . (d)-(g) show the quasiparticle spectral functions along the  $\Gamma$ -X direction at  $n=6.15$ . The color curves highlight the dominant orbital of the band, with  $d_{xz}/d_{yz}$  in red and  $d_{xy}$  in blue.

orbitally resolved quasiparticle spectral weight,  $Z_\alpha$ , as a function of the temperature (Fig. 4(c)), we show that the OSMP corresponds to the  $d_{xy}$  orbital being Mott localized ( $Z = 0$ ) and the rest of the  $3d$  orbitals remaining delocalized ( $Z > 0$ ). This result originates primarily from a combined effect of the orbital dependence of the projected density of states and the interplay between the Hund's coupling and crystal level splitting (see SI and Ref. 34).

To compare with the ARPES data, we have calculated the quasiparticle spectral function  $A(\mathbf{k}, E)$  in the 2-Fe BZ. At low temperature and in the non-interacting limit  $U=0$  (Fig. 4(d)), the electronic structure of the model agrees well with that of LDA, with the  $d_{xy}$  band deeper than the  $d_{xz}/d_{yz}$  band at X. This order switches with sufficiently strong interaction. At  $U=3.75\text{eV}$  (Fig. 4(e)), the  $d_{xy}$ -dominated bands are pushed above their  $d_{xz}/d_{yz}$  counterparts by the strongly orbital-dependent mass renormalization, as reflected in the orbital dependent quasiparticle spectral weights (Fig. 4(c)). The mass renormalization is the largest for the  $d_{xy}$  orbital ( $\sim 10$ ), and smaller for the  $d_{xz}/d_{yz}$  orbitals ( $\sim 3$ ), which is compatible with the low-temperature ARPES results (Fig. 1(e)). The temperature-induced crossover to the OSMP is clearly seen from the complete suppression of the spectral weights in the  $d_{xy}$  orbital that accompanies the moderate reduction of the weights in other orbitals (Fig. 4(c),(e)-(g)), in agreement with the ARPES results (Figs. 2 and 3).

The temperature-induced nature of the crossover con-

strains these AFS superconductors to be very close to the boundary of the OSMP in the zero temperature ground state, which is also the superconducting state. The best agreement between theory and experiments is achieved at  $U \sim 3.75\text{eV}$ . While the absolute value of this interaction is sensitive to the parameterization of the crystal levels and Hund's coupling, it is instructive to make a qualitative comparison with the case of the iron pnictides. The enhanced correlation effects for AFS tracks the reduction of the width of the ( $U=0$ )  $d_{xy}$  band, which is about 0.7 of its counterpart in 1111 iron arsenides.

One known concern for the AFS materials is the existence of mesoscopic phase separation into superconducting and insulating regions [35], which would both contribute spectral intensity in ARPES data. From measurement on an insulating RFS sample (Fig. S4(d)), we see negligible spectral weight and no well-defined dispersions within 0.1eV of  $E_F$ , as expected for an insulator. Hence, the insulating regions in the superconducting compounds do not contribute spectral weight to the near- $E_F$  energy range, in which the temperature-induced crossover is observed. In addition, superconducting gap consistent with previous reports [26, 28] is observed to open below  $T_C$  on the electron bands (see SI), confirming the origin of these observed bands to the superconducting regions of the sample. We have also measured a KFS sample whose resistivity is intermediate between superconducting and insulating (Fig. S4(b)), and was previously proposed to be semiconducting containing both metallic and insulating phases [36]. Interestingly, its  $d_{xz}/d_{yz}$  bands, which must come from the metallic phase, appear further renormalized by a factor of 1.3 compared with those of the superconducting compounds. In addition, we resolve small but finite spectral weight for a very shallow  $d_{xy}$  electron band near the X-point (Fig. S5(c)). As expected, the peak position is even closer to  $E_F$  compared with superconducting samples, consistent with further renormalization for the shallower  $d_{xy}$  band near X, which is harder to discern with temperature dependent study. These observations are consistent with the OSMP picture in that the metallic phase in this intermediate doping compound is likely even closer to the boundary of OSMP at low temperatures from the mass-diverging behavior of the  $d_{xy}$  bands. For the same interaction strength, calculation from our model also identifies the low temperature ground state of the superconducting, intermediate, and insulating phases to be located close to an OSMP, just at the boundary of an OSMP, and in a MI phase, respectively (see SI).

While we cannot completely rule out alternative explanations for the observations presented above (see SI), the consistency of the totality of the observations—including strongly orbital dependent band renormalization for  $d_{xy}$  versus  $d_{xz}/d_{yz}$  at both  $\Gamma$  and X in the low temperature metallic state, the non-trivial temperature-dependent spectral weight depletion for

only the  $d_{xy}$  band, systematic doping dependence of the related effects in the intermediate and insulating compounds—and the theoretical calculations makes this understanding a most likely scenario, suggesting that the superconductivity in this AFS family exists in close proximity to Mott behavior.

We thank V. Brouet, W. Ku, B. Moritz and I. Mazin for helpful discussions. ARPES experiments were performed at the Stanford Synchrotron Radiation Light-source and the Advanced Light Source, which are both operated by the Office of Basic Energy Science, U.S. DOE. The work at Stanford is supported by DOE Office of Basic Energy Science, Division of Materials Science and Engineering, under contract DE-AC02-76SF00515. The work at Rice has been supported by NSF Grant DMR-1006985 and the Robert A. Welch Foundation Grant No. C-1411. The work at Houston is supported in part by US Air Force Office of Scientific Research contract FA9550-09-1-0656, and the state of Texas through the Texas Center for Superconductivity at the University of Houston. MY thanks the NSF Graduate Research Fellowship Program for financial support.

- 
- [1] P.A. Lee, N. Nagaosa, and X.-G. Wen, *Rev. Mod. Phys.* 78, 17-85 (2006).
- [2] D.H. Lu *et al.*, *Nature* 455, 81 (2008).
- [3] W.L. Yang W. L. *et al.*, *Phys. Rev. B* 80, 014508 (2009).
- [4] M.M. Qazilbash *et al.*, *Nat. Phys.* 5, 647 (2009).
- [5] Z.P. Yin, K. Haule, and G. Kotliar, *Nat. Mat.* 10, 932-935 (2011).
- [6] A. Tamai *et al.*, *Phys. Rev. Lett.* 104, 097002 (2010).
- [7] Y. Lubashevsky, E. Lahoud, K. Chashka, D. Podolsky and A. Kanigel, *Nat. Phys.* 8, 309-312 (2012).
- [8] Z.K. Liu *et al.*, submitted.
- [9] T.J. Liu *et al.*, *Nat. Mat.* 9, 718-720 (2010).
- [10] J. Guo *et al.*, *Phys. Rev. B* 82, 180520(R) (2010).
- [11] A. Krzton-Maziopa *et al.*, *J. Phys.: Condens. Matter* 23, 052203 (2011).
- [12] C.-H. Li, B. Shen, F. Han, X. Zhu, and H.-H. Wen, *Phys. Rev. B* 83, 184521 (2011).
- [13] M.-H. Fang *et al.*, *Europhys. Lett.* 94, 27009 (2011).
- [14] H.-D. Wang *et al.*, *Europhys. Lett.* 93, 47004 (2011).
- [15] W. Bao *et al.*, *Chin. Phys. Lett.* 28, 086104 (2011).
- [16] Q. Si, and E. Abrahams, *Phys. Rev. Lett.* 101, 076401 (2008).
- [17] R. Yu, J.-X. Zhu, and Q. Si, *Phys. Rev. Lett.* 106, 186401 (2011).
- [18] Y. Zhou, D.-H. Xu, F.-C. Zhang, and W.-Q. Chen, *Europhys. Lett.* 95, 17003 (2011).
- [19] R. Yu, and Q. Si, *Phys. Rev. B* 84, 235115 (2011).
- [20] L. Craco, M.S. Laad, and S. Leoni, *Phys. Rev. B* 84, 224520 (2011).
- [21] M. Neupane *et al.*, *Phys. Rev. Lett.* 103, 097001 (2009).
- [22] V. Anisimov *et al.*, *Eur. Phys. J. B* 25, 191 (2002).
- [23] L. de' Medici, S.R. Hassan, M. Capone, and X. Dai, *Phys. Rev. Lett.* 102, 126401 (2009).
- [24] Y.-Z. You, F. Yang, S.-P. Kou, and Z.-Y. Weng, *Phys. Rev. B* 84, 054527 (2011).
- [25] S. J. Moon *et al.*, *Phys. Rev. B* 81, 205114 (2010).
- [26] Y. Zhang *et al.*, *Nat. Mat.* 10, 273-277 (2011).
- [27] T. Qian *et al.*, *Phys. Rev. Lett.* 106, 187001 (2011).
- [28] D. Mou *et al.*, *Phys. Rev. Lett.* 106, 107001 (2011).
- [29] I.A. Nekrasov, and M.V. Sadovskii, *JETP Lett.* 93, 166-169 (2011).
- [30] S. Graser *et al.*, *Phys. Rev. B* 81, 214503 (2010).
- [31] M. Yi, *et al.*, *PNAS* 108, 6878 (2011).
- [32] R. Yu, and Q. Si, *Phys. Rev. B* 86, 085104 (2012).
- [33] L. de' Medici, L., A. Georges, and S. Biermann, *Phys. Rev. B* 72, 205124 (2005).
- [34] R. Yu, and Q. Si, arXiv:1208.5547.
- [35] W. Li *et al.*, *Nat. Phys.* 8, 126-130 (2012).
- [36] F. Chen *et al.*, *Phys. Rev. X* 1, 021020 (2011).